Available online at www.sciencedirect.com
SCIENCE DIRECT®
Composites: Part B 36 (2005) 51–59
composites Part B: engineering
www.elsevier.com/locate/compositesb

Crystallization behaviour of new poly(tetramethyleneterephthalamide) nanocomposites containing SiO_2 fillers with distinct morphologies

Ana Catarina C. Esteves[a], Ana M. Barros-Timmons[a], J.A. Martins[b], W. Zhang[b], José Cruz-Pinto[a,*], Tito Trindade[a]

[a]*Departamento de Química, CICECO, Universidade de Aveiro, 3810-193 Aveiro, Portugal*
[b]*Departamento de Engenharia de Polímeros, IPC, Universidade do Minho, 4800-058 Guimarães, Portugal*

Received 1 June 2003; revised 5 December 2003; accepted 4 April 2004

Available online 28 May 2004

Abstract

Polyamide-based nanocomposites containing surface-modified SiO_2 nanofillers with different morphologies were prepared by in situ polymerisation. The nanocomposites microstructure was investigated by scanning electron microscopy, which showed a high degree of dispersion of the fillers. The isothermal crystallization kinetics, recorded with a differential scanning calorimeter, has shown a strong influence of the nanofillers morphology on the poly(tetramethyleneterephthalamide) crystallization behaviour. The strong nucleating effect of the inorganic substrate is interpreted as the combined result of a lower activation energy for the primary nucleation and a higher activation energy for the transport of chain stems to the growing lamellae.

Keywords: A. Polymer–matrix composites (PMCs); A. Nano-structures; B. Thermal properties; D. Thermal analysis

1. Introduction

Polymeric composite materials have since long attracted much interest, due to their potential applications in different fields, such as in automobile, house-hold, flame retardants, membranes and opto-electronic industries [1]. Even though polymers generally allow easy processing and are of relatively low cost compared to metal or ceramic materials, other inherent properties such as low modulus and/or low thermal stability have limited some of the applications. A successful strategy to overcome these drawbacks has been the insertion of inorganic fillers in the polymeric matrix, leading to the development of new promising composite materials [2].

In the last few years, polymer-based nanocomposites, which contain fillers of nanometric size, have been intensively investigated [3]. The properties of a polymer filled composite are mostly affected by the size, shape, composition, and state of agglomeration of the filler, and also by the degree of matrix-filler adhesion [4]. The use of nanoparticles as fillers provides a larger interfacial adhesion region that might result in considerably stronger interactions with the matrix and improvement of the final material. Additionally, nanofillers can confer unique properties to the nanocomposite, such as electric [5], optical [6,7], magnetic [8,9] or transport properties [10,11], which open a wealth of possibilities for future technological applications. Enhanced characteristics in polymer-based composites have so far been reported as a synergistic result from the combination of the individual component contributions [1–3]. In conventional composites, these improvements can be estimated through mixing rules, but they start to fail with nanocomposites, because interfacial interactions between components become extremely relevant in determining the bulk properties. Recent research has focused on possible mechanisms for the preparation of these type of materials, as well as on the phenomena occurring at the organic/inorganic interface [12–14]. Furthermore, some models for the interactions occurring between the two phases have also been developed [15,16].

Polyamides and the nylon series of thermoplastics constitute a family of compounds with extraordinary mechanical features. In fact, several polyamide-based nanocomposites with improved mechanical properties

* Corresponding author.
E-mail address: cpinto@dq.ua.pt (J. Cruz-Pinto).

1359-8368/$ - see front matter © 2004 Elsevier Ltd. All rights reserved.
doi:10.1016/j.compositesb.2004.04.005

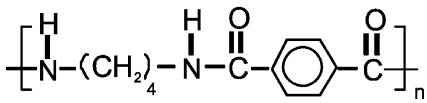

Fig. 1. Polymeric matrix: poly(tetramethyleneterephthalamide).

have recently been described in the literature. In these nanocomposites, different types of fillers were used such as, clays [17,18], and silicon oxide [19,20]. However, very few studies have reported the influence of the fillers on the thermal behaviour of the final nanomaterials [21,22].

Bearing this idea in mind, this work reports the synthesis and the thermal properties of new SiO_2/polyamide nanocomposites prepared by in situ polymerisation. The polymer used as matrix was poly(tetramethyleneterephthalamide) (Fig. 1), and has not yet been reported in literature for preparing this type of nanocomposites. The fillers were (i) SiO_2 spherical particles with average diameter of 275 ± 22 nm, (ii) SiO_2 spherical particles in the same diameter range but organically modified with a coupling agent (3-aminopropyltriethoxysilane, APS) and (iii) SiO_2 hollow fibres. The thermal properties were investigated by differential scanning calorimetry (DSC), with particular focus on the isothermal crystallisation and melting phase transitions. The influence of size, surface modification and morphology of the SiO_2 fillers on the crystallization behaviour of the polyamide is discussed.

2. Experimental

2.1. Synthesis

(i) *Spherical SiO_2 nanoparticles*. Spherical SiO_2 particles were prepared following the well-known Stöber method [23], with slight modifications. Tetraethoxysilane (TEOS, Aldrich 98%) (0.73 g) was added to a solution of absolute ethanol (Panreac, p.a.) (5 ml) and distilled water (0.06 g). The mixture was allowed to stand for 30 min. An aqueous solution of NH_4OH (Aldrich, 25% NH_3) (2 ml) was added dropwise to the ethanol solution and finally left to stand for another 30 min. The resulting SiO_2 was filtered under vacuum, washed thoroughly with distilled water to pH 8, and dried over silica gel.

The main vibrational modes of SiO_2 were identified in the FTIR spectra: ν_{O-H} (3467 cm^{-1}); ν_{Si-O} (1085 cm^{-1}); ν_{Si-OH} (955 cm^{-1}); $\delta_{Si-O-Si}$ (469 cm^{-1}) [24].

(ii) *Surface modification of spherical SiO_2 nanoparticles*. Following Foshiera et al. [25], some of the spherical SiO_2 fillers were submitted to an activation step at 700 °C, during 4 h, in order to increase the degree of de-hydroxylation of the silica surface. Activated silica (0.5 g) was dispersed in dry toluene (~3 ml) and APS (Aldrich 98%; 0.465 mmol) was added to the dispersion. The mixture was stirred at 110 °C for 22 h, under N_2. The solid was then filtered, washed with toluene and dried over silica gel. The IR spectrum did not show vestiges of non-bonded silane coupling agent. The amount of APS in the particles was determined by elemental analysis (1.6% (w/w), calculated in relation to the nitrogen content).

Scanning electron microscopy (SEM) analysis evidenced no changes in spherical SiO_2 nanoparticles morphology after activation. The SiO_2 absorption bands in FTIR vibrational spectra are very intense and it was not possible to identify the modes of APS in the spectra of the SiO_2 modified fillers. However, the absence of the band corresponding to the ν_{Si-OH} vibration mode and the ν_{Si-O} vibration band assigned to an higher wave number (1107 cm^{-1}) strongly indicate the disappearance of the silanol groups from the surface, and the possible existence of OR groups (R being a functional group) attached to the silicon atoms [24], respectively, confirming the derivatization of the SiO_2 spherical particles.

(iii) *SiO_2 fibres*. Hollow SiO_2 fibres were prepared following previous work of Mann et al. [26]. TEOS (0.73 g) was added to a solution of absolute ethanol (Panreac, p.a.) (5 ml), distilled water (0.06 g) and *dl*-tartaric acid (Aldrich 99%) (0.02 g). The mixture was allowed to stand for 30 min. After this, an aqueous solution of NH_4OH (2 ml) was added dropwise. The mixture was left to stand for 30 min. The precipitate was filtered through a metallic test sieve (400 mesh, Retsch) and washed thoroughly with water to remove the ammonium tartarate salt from the interior of the silica fibres as well as the small spherical aggregates formed. The solid was finally dried over silica gel. The FT infrared spectra of the solid retained in the filter showed the typical bands of SiO_2, whilst the bands due to the ammonium tartarate were not found.

The main vibrational modes of SiO_2 were here again identified in the FTIR spectra: ν_{O-H} (3451 cm^{-1}); ν_{Si-O} (1132 cm^{-1}); ν_{Si-OH} (953 cm^{-1}); $\delta_{Si-O-Si}$ (471 cm^{-1}) [24].

Poly(tetramethyleneterephthalamide). An aqueous solution of 1,4-diaminobutane (Aldrich, 99%) (1.58 g, 7.5 mmol) in de-ionised water (40 ml) containing Na_2CO_3 (1.58 g) was vigorously stirred in a glass beaker (600 ml) with a domestic blender. To this mixture, a solution of terephthaloyl chloride (Aldrich, 98%) (10.1 g, 7.5 mmol) in chloroform (Merck, p.a.) (16 ml) was rapidly added under vigorous stirring. A white precipitate was immediately formed. De-ionised water (200 ml) was added and the vigorous stirring was kept for 15 min. The mixture was left under magnetic stirring for 30 min to promote the complete reaction and to wash the precipitate. The polyamide was filtered and washed thoroughly with water, and then dried under vacuum for 3 days.

The polymer was characterized by FTIR and the bands were assigned to the vibrational modes of the respective monomers used. The average molecular weight ($\bar{M}_v$) of the poly(tetramethyleneterephthalamide) was determined by dilute solution viscometry. Measurements were performed on *m*-cresol solutions at 25 °C. $\bar{M}_v = 51.324$ g/mol was calculated using the Mark-Houwink constants reported in

the literature for nylon 6,6 for these analytical conditions ($a = 0.61$ and $K = 240 \times 10^{-3}$ ml/g) [27].

SiO_2/poly(tetramethyleneterephthalamide) nanocomposites. The nanocomposites were prepared by in situ polymerisation in the presence of the inorganic fillers, following the procedure described for the polymeric matrix. The prepared SiO_2 fillers were dispersed in the aqueous solution before adding any other reagent (10% wt relative to the total mass of monomers used). The nanocomposites were filtered, washed with water and dried under vacuum for three days. The solids evidenced a homogeneous appearance and no signs of macroscopic segregation. The nanocomposites were characterized by FTIR and the bands were assigned to the vibrational modes of the respective monomers used. It was not possible to identify the vibrational modes attributed to the fillers, as the polymer bands were very broad and strong. The nanocomposites studied in this work are listed in Table 1.

2.2. Instrumentation

The infrared spectra were recorded on a Matson 700 FTIR spectrometer using dry KBr disks. The BET surface area of the SiO_2 fillers (m^2/g) were determined in a Gemini 2370 V5.00 equipment. The analysis was carried out at room temperature with approximately 0.3 g of each sample, using N_2 as adsorbing gas and with a flow of He as evacuating gas. Elemental analysis was determined in the microanalysis laboratory of the University of Santiago de Compostela.

SEM images were collected with a FEG-SEM Hitachi S4100 microscope operating at 25 kV. The samples for microscopy were prepared by dispersing a small amount of the nanoparticles in ethanol. A drop of the suspension was deposited on aluminium plates and then coated with evaporated carbon. The nanocomposites were directly deposited as synthesized onto the aluminium plates and then coated with evaporated carbon. The SiO_2 content (%) was determined by calcination of the samples in a tubular oven at 800 °C, during 4 h, under an air stream. The error estimated for this calculation was approximately ±4.8%, considering the calcination of the PA0 sample.

DSC experiments. A Perkin Elmer DSC-7 (Norwalk, CT) running in standard mode was used. The temperature of the cold block was kept at 5 °C and the nitrogen purge gas flow rate was 20 cm^3/min. Temperature and enthalpic calibrations were carried out according to the DSC7 Perkin Elmer Manual procedures. For the isothermal experiments the temperature calibration was performed at 0.1 °C/min and checked before and after a set of experiments. Deviations of ±0.2 °C for the measured onset were obtained, and it will be assumed that this is the temperature error for the crystallization experiments carried out in these conditions.

The sample weight (accurately measured to within 10^{-3} mg) was around 10 mg for all materials analysed and 50 μl aluminium pans with holes were used. For evaluating the melting range, previous heating experiments were performed over all samples, from 30 to 300 °C, at a heating rate of 20 °C/min. For these experiments, a base line was obtained with two empty pans, in the same working temperature range and with the same scanning rate. The isothermal experiments were performed according to the following temperature program: the sample was heated up to 300 °C and, after the stabilization of the heat-flow signal, an additional 1 min residence time was allowed at the start temperature; the sample was then cooled down to the crystallization temperature at a controlled cooling rate of −60 °C/min; a long enough dwell time was allowed at this temperature, for recording the entire crystallization process. When necessary, especially for samples crystallized at lower temperatures, a blank experiment was performed to eliminate the transient due to the temperature jump from the starting temperature to the crystallization temperature, and to allow a better definition of the zero crystallization time (the start of the isothermal).

Table 1
SiO_2/poly(tetramethyleneterephthalamide) nanocomposites

Sample	SiO_2 filler	BET surface area of the fillers (m^2/g)	Polymer matrix	SiO_2 (w/w%)
PA0	–	–	Poly(tetramethylene-terephthalamide)	–
PA1	Spherical particles ($\bar{D} = 275 \pm 22$ nm)	13.3795	Poly(tetramethylene-terephthalamide)	–
PA2	Spherical particles ($\bar{D} = 275 \pm 22$ nm)	10.0514	Poly(tetramethylene-terephthalamide)	11.4
PA3	Hollow fibres ($L < 150$ μm)	6.1981	Poly(tetramethylene-terephthalamide)	15.2

3. Results and discussion

Many authors have reported the preparation of SiO_2/polyamide nanocomposites as potential materials for technological applications, namely as flame-retardants [28] and films [29]. Generally, the preparation methods involve the simple mixing of the components, which may result in a low degree of dispersion of the fillers in the polymer matrix. In this work, the polymer nanocomposites were prepared by in situ polymerisation in order to promote a good dispersion of the nanoparticles within the polymer matrix. For some of the fillers the surface was modified with a coupling agent bearing an organic group, to increase the compatibility with the polymer matrix. The SEM images of the fillers used are shown in Fig. 2.

For the SiO_2 spherical particles, a nearly monodisperse sample was obtained with diameters of 275 nm (Fig. 2a) and a standard deviation of ±8%. As to the fibres, hollow

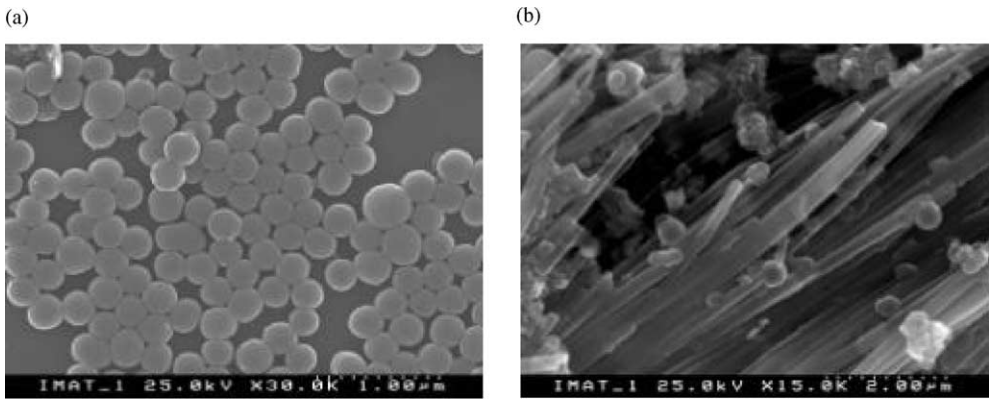

Fig. 2. SEM images of SiO_2 fillers: (a) spherical particles; (b) hollow fibres.

SiO_2 fibres with a length lower than 150 μm were synthesized. Although a few spherical aggregates were still present in this sample after filtration, the analysis of several images showed that the hollow fibres were the predominant morphologies in these samples (Fig. 2b).

The SEM images of the nanocomposites prepared (Fig. 3a and b), show that the fillers are reasonably well dispersed in the polymeric matrix. Nevertheless, some aggregates at the surface of the polymer were also identified. The polymerisation reaction involved in the preparation of the nanocomposites occurred almost instantaneously, after mixing the solutions containing the monomers, and this may preclude a complete homogeneous dispersion of the fillers in the matrix. However, the organic modification of the SiO_2 spherical particles with the coupling agent APS, seems to improve the dispersion of the fillers in the polyamide matrix. Yang et al. [30] described similar results for SiO_2/Nylon 6 nanocomposites, in which the nanoparticles pre-modified with aminobutiric acid disperse more homogeneously in the polymeric matrix compared to the fillers which were not surface-modified.

3.1. Crystallization kinetics studies

For identifying the melting temperature range of the different materials, heating scans were performed at 20 °C/min, under the conditions described in the experimental part of the work. These scans were performed after a controlled cooling at the same rate, so the results obtained are representative of the selective melting of the crystalline regions developed in the different samples. Fig. 4 shows the results obtained for the materials analysed. As it may be observed from these results, the incorporation of inorganic fillers increases the sample melting temperature. The samples showing higher melting temperatures and sharper peaks are PA2-(SiO_2/APS)/poly(tetramethyleneterephthalamide) and PA3-SiO_2 hollow fibres/poly(tetramethyleneterephthalamide).

For a better characterization of the material, its thermodynamic melting temperature was evaluated using the Hoffman and Weeks graphical procedure. The samples were crystallized at different temperatures and their melting was evaluated through measurements of the onset and peak values for scans carried out at heating rates of 20 and 60 °C/min. Similar results were obtained for both situations and they are shown in Fig. 5. Some representative values measured for the onset and peak temperatures, and also the values of the enthalpy of fusion for the sample PA0 are given in Table 2.

No reference to this material (poly(tetramethyleneterephthalamide)) was found in the literature, but the value obtained for the thermodynamic melting temperature

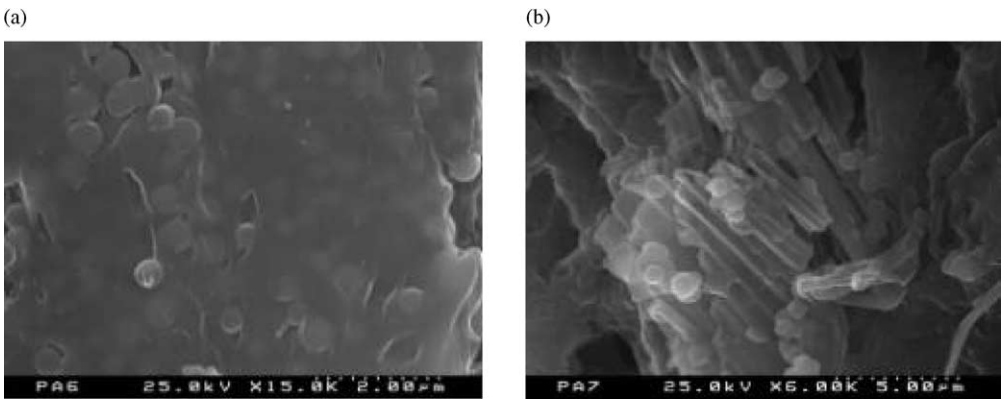

Fig. 3. SEM images of the nanocomposites: (a) PA2: (SiO_2/APS)/poly(tetramethyleneterephthalamide); (b) PA3: SiO_2 hollow fibres/poly(tetramethyleneterephthalamide).

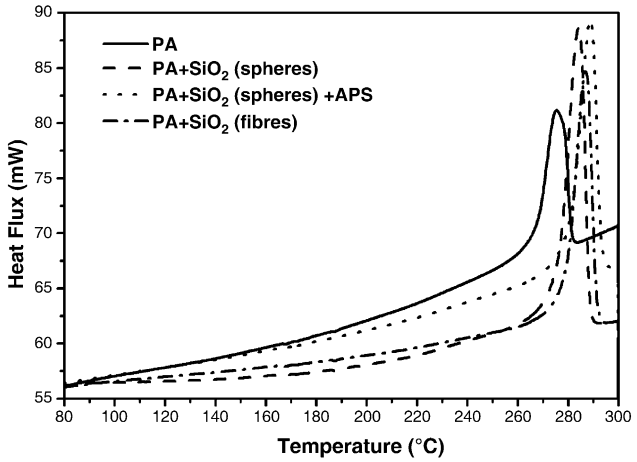

Fig. 4. Melting of the different sample's materials recorded in the DSC with a heating rate of 20 °C/min after controlled cooling at the same rate. The sample weight is around 10 mg for all samples.

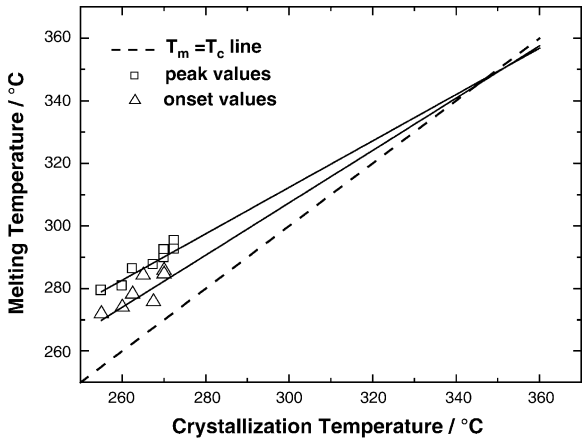

Fig. 5. Hoffman and weeks plot for evaluating the thermodynamic melting temperature of the sample PA0. The heating scans leading to the results shown were performed at 20 °C/min. Different samples were used in the scans, all of them with mass around 10 mg. The evaluated thermodynamic melting temperature, T_m^0, is 347 °C.

(347 °C, both for the onset and peak extrapolated values) is acceptable when compared with the value reported for the melting temperature of poly(hexamethyleneterephthalamide) that is 371 °C [27]. As for the glass transition temperature, attempts to measure its value from DSC experiments failed, and a value of 11.4 °C was estimated from a group interaction modelling method (GIM), as described in Appendix A.

Table 2
Onset (T_0) and peak (T_p) temperatures measured for samples of PA0 crystallized at the indicated temperatures

T_c (°C)	T_0 (°C)	T_p (°C)	Δh/ (J g^{-1})
255	270.1	279.4	47.1
260	274.0	281.8	50.9
265	278.2	286.9	52.5

The enthalpy of fusion is also shown. Scans performed at 20 °C/min and sample masses around 10 mg.

Since the melting experiments were performed over samples cooled under controlled conditions, the results of Fig. 4 suggest that the inorganic nanocomposites may act as nucleating agents during the solidification process. This assumption will be analysed below.

The results of Fig. 6 show the different steps leading to the isothermal experiments: the residence time of 1 min at the start temperature, the cooling to the crystallization temperature (showing the transient due to the cooling process) and the dwell time at the crystallization temperature. For PA0 the crystallization temperature is 260 °C and for all the other samples, it is 270 °C. It is observed that the crystallization peak is successively shifted to lower crystallization times for the samples with SiO_2 spherical particles (PA1), SiO_2 spherical particles derivatized with APS (PA2), and for SiO_2 hollow fibres

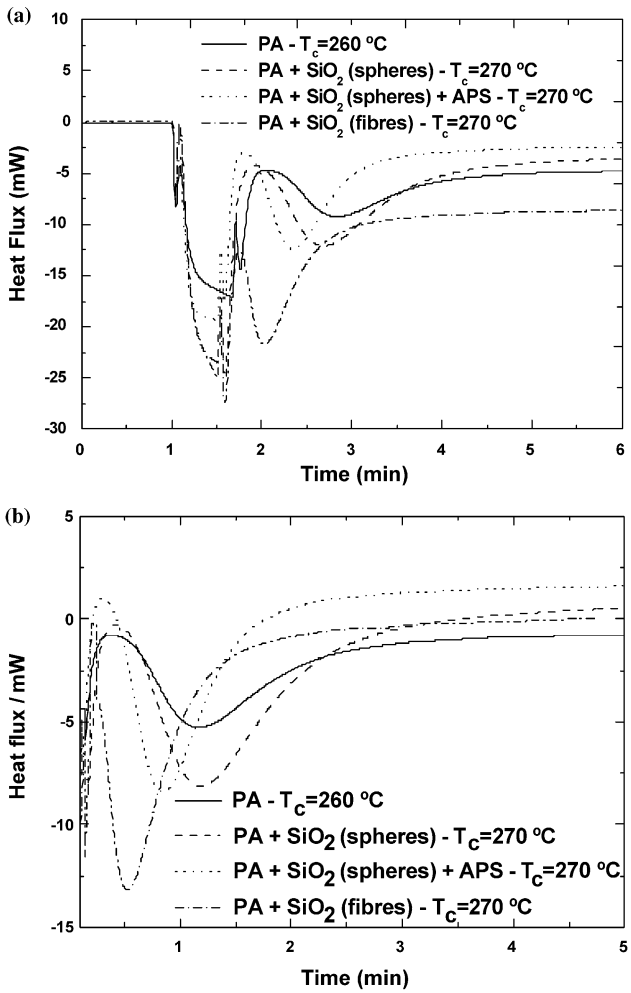

Fig. 6. Isothermal crystallization experiments for the different samples used at 260 °C for PA0 and at 270 °C for PA1, PA2 and PA3. The curves shown in (a) are not subtracted of the blank run to eliminate the transient due to the jump from the initial temperature to the crystallization temperature. The curves subtracted from the blank (b) were used for evaluating the crystallization kinetics.

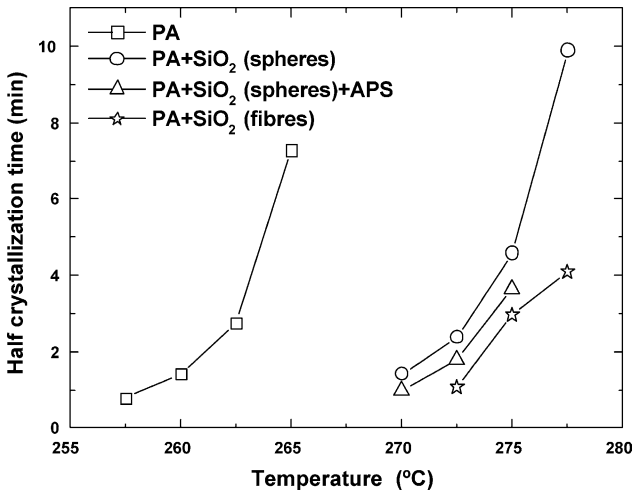

Fig. 7. Values of the reciprocal half-crystallization time against the crystallization temperature for the samples prepared in this work.

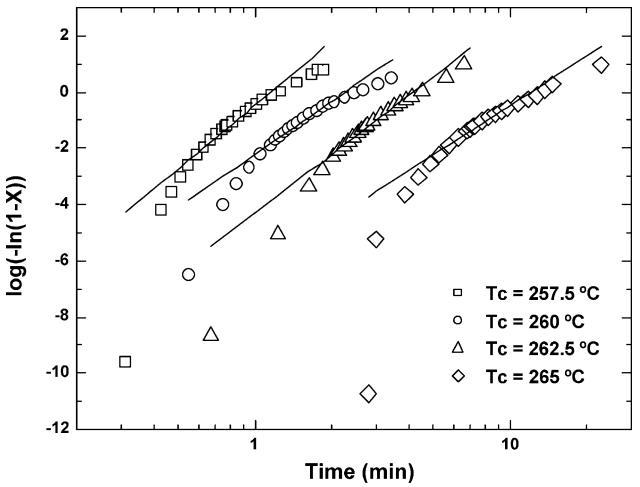

Fig. 8. Avrami plot for the isothermal crystallization of the PA0 sample at the indicated temperatures. The full line is the fitting obtained with Avrami's equation.

(PA3), indicating a more intense nucleation activity for the sample with SiO_2 fibres (PA3).

Fig. 6b shows the same results after blank subtraction (to eliminate the transient, heat capacitive effects during cooling to the crystallization temperatures) and zero time correction (to set the start of the isothermal period).

The nucleating effect of the fillers may be further and quantitatively evaluated by the results of Fig. 7, where the half-crystallization time is plotted against different crystallization temperatures. Assuming that the inorganic agents do not affect the polymer thermodynamic melting temperature, it may be seen from the results of Fig. 7, for the same half-crystallization time, the supercooling decreases from the PA0 sample (simple polyamide) to PA3 (polymer with SiO_2 fibres). These results also clearly show the effect of the morphology of the inorganic fillers on the overall crystallization kinetics. For the PA1 sample, with SiO_2 spherical particles, a sudden increase of the nucleation activity is observed in comparison with PA0. The nucleating activity effect increases for PA2, where surface derivatization of the SiO_2 spherical particles by the APS contributes for the enhancement of the nucleation. As expected, this effect is further enhanced for PA3, due to the geometry of the inorganic fillers.

The isothermal crystallization kinetics of the different samples was analysed on the basis of Avrami's overall crystallization equation

$$X(t) = 1 - \exp(-kt^n), \tag{1}$$

where $X(t)$ is the crystallinity (relative to the maximum attained value at infinite time), k is a kinetic constant proportional to the nucleation density and to the growth rate raised to the power n (for instantaneous nucleation), where n is determined by the dimensionality and nucleation type of the growing semicrystalline spherulitic structures.

The results obtained for PA0 are presented in Fig. 8 and the values of the parameters obtained for all materials are in Table 3. The values obtained for parameter n are near 3, thus showing that the nucleation may be assumed to be instantaneous and that the developed semicrystalline structures have an approximate spherical shape (spherulites).

From the values of the parameters shown in Table 3, it is difficult to extract additional information related to the nucleation activity for the different nanocomposite morphologies. However, an analysis of the temperature dependence of the kinetic parameter (k) may provide further additional information related to the nucleation process in the different samples [31]. Since, for instantaneous nucleation, k is proportional to the average nucleation density and to the cube of the spherulite radial growth rate, it is important to account for the individual temperature dependence of these two parameters.

The temperature dependence of the spherulite growth rate is assumed to be the one given by the Lauritzen and Hoffman equation for the secondary nucleation

$$G = G_0 \exp\left(-\frac{\Delta G_d}{k_B T}\right)\exp\left(-\frac{K_G}{T\Delta T f}\right), \tag{2}$$

where ΔG_d is the activation Gibbs free energy for transport and K_G is equal to $4b\sigma\sigma_e T_m^0/k_B\Delta h_m$; b is the thickness of a chain stem, σ and σ_e are the lateral and folding surface energies, k_B is the Boltzmann's constant, f a factor which accounts for the decrease of the enthalpy of fusion (Δh_m) with the crystallization temperature and ΔT is the supercooling (difference between the thermodynamic melting temperature (T_m^0) and the crystallization temperature).

In most treatments of the kinetic constant obtained from Avrami's equation for the overall crystallization kinetics, it is assumed that, for instantaneous nucleation, the nucleation density is constant, independent of the crystallization temperature. It was shown previously that, if this temperature dependence is considered [32] even in an approximate way, it is possible to relate the data from

Table 3
Values of the kinetic constant (k) and Avrami exponent (n) obtained for Avrami's equation

T_c (°C)	PA0		PA1		PA2		PA3	
	k (s^{-n})	n	k (s^{-n})	n	k (s^{-n})	n	k (s^{-n})	n
257.5	2.17×10^{-4}	3.27	–	–	–	–	–	–
260	3.25×10^{-4}	2.74	–	–	–	–	–	–
262.5	1.36×10^{-5}	3.01	–	–	–	–	–	–
265	1.39×10^{-5}	2.52	–	–	–	–	–	–
270	–	–	1.37×10^{-4}	2.94	1.92×10^{-4}	3.12	–	–
272.5	–	–	3.07×10^{-5}	2.93	5.60×10^{-5}	2.98	3.39×10^{-4}	2.92
275	–	–	4.16×10^{-6}	2.95	5.51×10^{-7}	3.45	5.71×10^{-5}	2.93
277.5	–	–			–	–	1.44×10^{-5}	2.78

the local crystallization kinetics, as the growth rate, with the information obtained from the overall crystallization kinetics, as the reciprocal half-crystallization time or the kinetic constant of Avrami's equation. This relationship enables the prediction of the average nucleation density (or the average spherulite size).

The temperature dependence of the average nucleation density may be established by assuming that primary nucleation is coherent and that is instantaneous. An approximate expression for its temperature dependence is

$$\bar{N} = N_s \exp\left(-\frac{\Delta G_N}{k_B T}\right) = N_s \exp\left(-\frac{K_N}{T\Delta T f}\right), \quad (3)$$

where ΔG_N is the activation Gibbs free energy for the formation of an embryo with critical size, K_N is, under the above assumptions, equal to K_G of Eq. (2), and N_s is the total number of chain segments in an ideal mixture with embryos.

Assuming, in addition, that the nucleated particles quickly acquire an approximate spherical shape, the kinetic constant of Avrami's equation, Eq. (1), may be written, from Eqs. (2) and (3), as

$$(k)^{1/3} = (c\bar{N})^{1/3} G = (cN_s)^{1/3} G_0 \exp\left(-\frac{\Delta G_d}{k_B T}\right) \exp\left[-\frac{1}{T\Delta T f}\left(\frac{K_N + 3K_G}{3}\right)\right], \quad (4)$$

where c is a constant equal to a product of a geometrical shape factor of the growing semicrystalline entity by the density ratio between the solid and liquid phases.

The slope of a line in a graph of $\ln(k)^{1/n}$ against $(1/T\Delta T f)$ is then proportional to the surface energies for primary and secondary nucleation. Since the latter energies should be the same for all samples, the differences in the slopes may only be ascribed to the different surface energies of the primary nucleation process. As to the value of the intercept ($\ln k_0$), it is proportional to $\ln(N_s)^{1/3} - \Delta G_d/k_B T$. The values obtained for the slope $K_g = (K_N + 3K_G/3)$ and for k_0 are in Table 4.

From the results of Table 4 it is possible to conclude that the lower values (with respect to the PA0 sample) obtained for the slope K_g of samples PA1, PA2 and PA3 may only be explained by the lower values of the surface energies presented by these samples for the primary nucleation process. This conclusion is consistent with the results of Fig. 7, which show that the inorganic fillers act as nucleation sites for the crystallization. As explained previously, k_0 is proportional to the number of chain stems to be added to an embryo and to the activation energy for the transport of a chain stem to the surface of a growing lamellae. Since the crystallization of samples PA1, PA2 and PA3 occurs at higher temperatures, it is expected that N_s per unit volume of the sample, will be smaller than for sample PA0. On the other hand, it could also be argued that the inorganic fillers may hinder chain mobility, thereby increasing the activation energy for transport. These two factors may explain the results obtained for k_0.

Sample PA2 (SiO_2 spherical particles derivatized with APS) presents an unexpected behaviour for K_g and k_0. As shown in Fig. 7, the crystallization kinetics for this sample is faster than for sample PA1, but the values of Table 4 indicate an increase of the values obtained for the above two parameters. During the derivatization process only part of the APS molecules are attached to the SiO_2 surface. The remaining part of the molecule is free to interact with the polymer matrix. As a result of this interaction we assume that the activation energy for transport will decrease, thus facilitating the movement of the chain stems to the growing lamellae. On the other hand, the molecules attached to the SiO_2 surface will make more

Table 4
Values obtained for K_g and k_0 from a plot of $\ln(k)^{1/n}$ against $(1/T\Delta T f)$

Sample	K_g/K^{-2}	$k_o/m.s^{-1}$
PA0	1.22×10^6	24.25
PA1	9.28×10^5	20.52
PA2	1.03×10^6	23.82
PA3	8.56×10^5	19.73

The values used for the thermodynamic melting temperature and glass transition temperature were indicated in the text and it was assumed that the transport term of the growth rate has a WLF functionality, $\Delta G_d = C_1 C_2/(C_2 + T - T_g)$, with $C_1 = 25$ and $C_2 = 30$ K.

difficult the formation of primary nuclei, thereby contributing to the observed increase of the surface energies for primary nucleation. The relatively faster crystallization kinetics observed for this sample may then be ascribed to assumed lower activation energy for the transport of the chain stems to the growing lamellae.

However, a positive, final, conclusion on this respect may require a detailed rheological analysis of the polymer melts for the different samples, as well as an analysis of the effect of the nanofillers on the polymer's glass transition temperature.

4. Conclusions

This is the first report on the influence of surface-modified SiO_2 *nano*fillers with different morphologies on the thermal behaviour of polyamide-based nanocomposites. A high degree of dispersion of the fillers in the final nanocomposites was obtained by using the in situ polymerisation process. The nanofillers strongly influence the thermal (namely the crystallization) behaviour of the polymer matrices, their effect showing a bulk (rather than merely a surface) nature. The nucleation density and the overall crystallization rates are very significantly increased, and the results may be quantitatively interpreted by current polymer crystallization theories.

Acknowledgements

A.C. Esteves thanks the University of Aveiro for a research grant. This work was financed by the Portuguese Foundation of Science and Technology (FCT) (Project POCTI/35458/CTM/2000 co-financed by FEDER). The Portuguese Foundation of Science and Technology (FCT) is also acknowledged for the grants BSAB/309/2002 assigned to J.A. Martins, and for the grant BPD/5517/2001 assigned to W. Zhang.

Appendix A

The value of the glass transition temperature used for estimating the values of Table 4 was predicted from the GIM applied to the poly(tetramethyleneterephtalamide).

Following the nomenclature used by Porter [32], the values obtained for the zero order and first order connectivity indexes are, respectively, ${}^0\chi = 11.38$, ${}^0\chi^v = 8.95$, ${}^1\chi = 7.77$ and ${}^1\chi^v = 5.44$, from which the cohesion energy may be evaluated. The value obtained for it was $E_{coh} = 66.034$ kJ/mol. Assuming for the temperature characterising the vibrations in the chain axis $\theta_1 = 550$ K, and the number of skeletal modes as $N = 21$, the value predicted for the glass transition temperature is 11.4 °C.

References

[1] Seymour RB. Polymer composites-new concepts in polymer science. Netherlands: VSP Ultecht; 1990.
[2] Yang BZ. Advanced polymer composites: properties and applications. Materials Park: ASM International; 1994.
[3] Special edition: Organic–inorganic nanocomposite materials. Chem Mater 2001; 13(10).
[4] Shalim RE. Polymer matrix composites. London: Chapman & Hall; 1995.
[5] Woggon U, Bogdanov SV, Wind O, Schlaad KH, Pier H, Klingshirn C, Chatziagorastou P, Fritz HP. Electro-optic properties of CdS embedded in a polymer. Phys Rev B 1993;48(16):11979–86.
[6] Rajeshwar K, Tacconi NR, Chenthamarakshan CR. Semiconductor-based composite materials: preparation, properties and performance. Chem Mater 2001;13:2765–82.
[7] Esteves ACC, Monteiro OC, Barros-Timmons AMV, Boemare C, Soares MJ, Monteiro T, Trindade T. Optical properties of the synthetic nanocomposites SiO_2/CdS/poly(styrene-*co*-maleic anhydride) and SiO_2/CdS/poly(styrene-*co*-maleimide). J Nanosci Nanotechnol 2002;2:177–81.
[8] Burke NAD, Stöver HDH, Dawson FP. Magnetic nanocomposites: preparation and characterization of polymer-coated iron nanoparticles. Chem Mater 2002;14:4752–61.
[9] Ramos J, Palacio F. Production of magnetic nanoparticles in a poly(vinyl pyridine) matrix. Polymer 2000;41:8461–4.
[10] Joly C, Smaihi M, Porcar L, Noble RD. Polyimide-silica composite materials: how does silica influence their microstructure and gas permeation properties? Chem Matter 1999;11:2331–8.
[11] Bharadwaj RK. Modeling the barrier properties of polymer-layered silicate nanocomposites. Macromolecules 2001;43(26):9189–92.
[12] Schmidt D, Shah D, Gianellis P. New advances in polymer layered silicate Nan composites. Curr Opin Solid State Chem 2002;6:205–12.
[13] Kim GM, Lee DH, Hoffman B, Kressler J, Stoppelamnn G. Influence of nanofillers on the deformation process in layered silicate/polyamide-12 Nan composites. Polymer 2001;42:1095–100.
[14] Jang J, Park H. Formation and structure of polyacrylamide-silica nanocomposites by sol–gel process. J Appl Polym Sci 2002;83:1817–23.
[15] Ginzburg VV, Balazs AC. Three-dimensional simulations of diblock copolymer/particle composites. Polymer 2002;43:461–6.
[16] Nowicki W. Structure and entropy of long polymer chain in the presence of nanoparticles. Macromolecules 2002;35(4):1424–936.
[17] Bureau MN, Denault J, Cole KC, Enright GD. The role of crystallinity and reinforcement in the mechanical behaviour of polyamide-6/clay nanocomposites. Polym Eng Sci 2002;42(9):1897–906.
[18] Okamoto M, Morita S, Kotaka T. Dispersed structure and ionic conductivity of smectic clay/polymer Nan composites. Polymer 2001;42:2685–8.
[19] Ou Y, Yang F, Yu ZZ. A new conception on the toughness of nylon 6/silica nanocomposite prepared via in situ polymerization. J Polym Sci: Part B 1998;36:789–95.
[20] Zyl WE, García M, Scrauwen AG, Kooi BJ, Hosson JTM, Verweij H. Hybrid polyamide/silica nanocomposites: synthesis and mechanical testing. Macromol Mater Eng 2002;287:106–10.
[21] Bershtein VA, Egorova LM, Yakushev PN, Pissis P, Sysel P, Brozova L. Molecular dynamics in nanostructured and polyimide-silica hybrid materials and their thermal stability. J Polym Sci 2002;40:1056–68.
[22] Zhu J, Uhl FM, Morgan AB, Wilkie CA. Studies on the mechanism by which the formation of nanocomposites enhances thermal stability. Chem Mater 2001;13(12):4649–54.
[23] Stöber W, Fink A, Bohn E. Controlled growth of monodisperse silica spheres in the micron size range. J Colloid Interface Sci 1968;26:62–9.
[24] Nakamoto K. Infrared an raman spectra of inorganic and coordination compounds, 5th ed. New York: Wiley; 1997.

[25] Foshiera JL, Pizzolato TM, Benvenutti EV. FTIR thermal analysis on organofunctinalized silica gel. J Braz Chem Soc 2001;12(2):159–64.
[26] Mann S, Miyaki F, Davis SA, Charmant JPH. Organic crystal templating of hollow silica fibers. Chem Matter 1999;11(11):3021–4.
[27] Branddrup J, Immergut EH, Grulke EA. Polymer handbook, 4th ed. New York: Wiley; 1998.
[28] Liu J, Gao Y, Wang F, Wu M. Preparation and characteristics of nonflammable polyimide materials. J Appl Polym Sci 2000;75: 384–9.
[29] Chen Y, Iroh O. Synthesis and characterization of polyimide/silica hybrid composites. Chem Mater 1999;1:1218–22.
[30] Yang F, Ou Y, Yu Z. Polyamide 6/silica nanocomposites prepared by in situ polymerisation. J Appl Polym Sci 1998;69:355–61.
[31] Martins JA, Cruz Pinto JJC. Evaluation of the instantaneous nucleation density in the isothermal crystallization of polymers. Polymer 2002;43:3999–4010.
[32] Porter D. Group interaction modelling of polymer properties. New York: Marcel Dekker; 1995.